Site-specific colloidal crystal nucleation by template-enhanced particle transport

Chandan K. Mishra[a,1], A. K. Sood[b,c], and Rajesh Ganapathy[c,d,1]

[a]Chemistry and Physics of Materials Unit, Jawaharlal Nehru Centre for Advanced Scientific Research, Jakkur, Bangalore 560064, India; [b]Department of Physics, Indian Institute of Science, Bangalore 560012, India; [c]International Centre for Materials Science, Jawaharlal Nehru Centre for Advanced Scientific Research, Jakkur, Bangalore 560064, India; and [d]Sheikh Saqr Laboratory, Jawaharlal Nehru Centre for Advanced Scientific Research, Jakkur, Bangalore 560064, India

Edited by David A. Weitz, Harvard University, Cambridge, MA, and approved September 6, 2016 (received for review May 27, 2016)

The monomer surface mobility is the single most important parameter that decides the nucleation density and morphology of islands during thin-film growth. During template-assisted surface growth in particular, low surface mobilities can prevent monomers from reaching target sites and this results in a partial to complete loss of nucleation control. Whereas in atomic systems a broad range of surface mobilities can be readily accessed, for colloids, owing to their large size, this window is substantially narrow and therefore imposes severe restrictions in extending template-assisted growth techniques to steer their self-assembly. Here, we circumvented this fundamental limitation by designing templates with spatially varying feature sizes, in this case moiré patterns, which in the presence of short-range depletion attraction presented surface energy gradients for the diffusing colloids. The templates serve a dual purpose: first, directing the particles to target sites by enhancing their surface mean-free paths and second, dictating the size and symmetry of the growing crystallites. Using optical microscopy, we directly followed the nucleation and growth kinetics of colloidal islands on these surfaces at the single-particle level. We demonstrate nucleation control, with high fidelity, in a regime that has remained unaccessed in theoretical, numerical, and experimental studies on atoms and molecules as well. Our findings pave the way for fabricating nontrivial surface architectures composed of complex colloids and nanoparticles as well.

self-assembly | colloids | surface growth | graded energy surfaces | depletion

Realizing ordered surface nano- and microstructures of well-defined size and shape from the autonomous assembly of their constituent building blocks remains one of the key challenges in materials science (1–4). With regard to atomic/molecular surface assembly, using templates that preferentially enhance crystal nucleation events at specific sites is a proven approach toward realizing mesoscopically ordered structures like quantum dot arrays and supramolecular nanoassemblies (5, 6). Extending this technique to tailor surface structures composed of nanoparticles and colloids is highly desirable for applications that include sensors, structural color-based filters, and optoelectronic devices (7–9). Although recent experiments find that colloidal and atomic thin-film growth on homogeneous surfaces obeys identical scaling laws (10, 11), translating concepts gleaned from site-specific nucleation studies on atoms/molecules to colloids is anything but easy. To achieve site-specific nucleation with high fidelity, the particles' surface mean-free path, L, should be larger than the distance between the preferential nucleating sites L_p. In conventional surface growth studies, L is set by the ratio of the monomer surface diffusion constant to its deposition flux D/F with $L \sim (D/F)^{1/6}$ for $D/F > 10^4$ (4, 12). For atoms, a broad window of D/F values spanning $10^{-1} - 10^9$ can be readily accessed and thus, L can be easily tuned to be larger than L_p. However, for colloids, owing to their large size, D is small and the D/F window is limited to $10^{-1} - 10^4$. To further complicate matters, over this window, simulations, atomic and colloid experiments find deviations from mean-field scalings and L, or equivalently the island density, is found to saturate with decreasing D/F (4, 10). In fact. for micrometer-sized colloids, the maximum L is $\sim 5 - 7$ particle diameters only. Consequently, it is as yet unclear whether site-specific nucleation is even a viable strategy to fabricate mesoscopically organized structures made of nano- and microscale particles. This has resulted in numerous alternate approaches that include selective evaporation (13–16) and external field-driven assembly (9, 17–20) to help realize the target structures. Many of these techniques, however, are often particle specific and do not allow exquisite control over the nucleation and growth process.

Results and Discussion

Enhancing Particles' Mean-Free Path. A plausible route to help alleviate the restrictions on L, imposed by D/F, is to use surfaces with energy gradients to transport particles to desired locations. Using the facile replica imprinting technique (21), we present a design principle based on templates with spatially varying feature sizes which in the presence of short-range depletion attraction induced activation energy gradients for the diffusing colloids. Our substrates comprised linear and square moiré patterns on polymethylmethacrylate (PMMA) layers spin-coated on glass coverslips. We fabricated these patterns, by first transferring a linear (square) array of trenches (holes), with periodicity λ, from a master grating to the PMMA substrate (8). This was followed by a second imprint at an angle θ, relative to the first, which resulted in a long wavelength modulation of the trench (hole) depths (*Materials and Methods*). Whereas λ decides the symmetry of the growing crystallites, the

Significance

The deliberate positioning of nano- and microstructures on surfaces is often a prerequisite for fabricating functional devices. Whereas template-assisted nucleation is a promising route to self-assemble these structures, its success hinges on particles reaching target sites prior to nucleation. Thus, for larger building blocks like nanoparticles and colloids, the low surface mobilities impose an impractical upper bound on the maximum achievable separation between surface features. Here, we engineered surfaces with energy gradients that not only aided in transporting particles to target sites but also dictated the size and symmetry of the growing crystallites. Remarkably, the enhancement in particles' surface mean-free path allows control over nucleation density in a regime that cannot be accessed in conventional template-assisted growth.

Author contributions: C.K.M., A.K.S., and R.G. designed research; C.K.M. performed research; C.K.M. contributed new reagents/analytic tools; C.K.M., A.K.S., and R.G. analyzed data; and R.G. wrote the paper.

The authors declare no conflict of interest.

This article is a PNAS Direct Submission.

[1]To whom correspondence may be addressed. Email: mishrachandan23@gmail.com or rajeshg@jncasr.ac.in.

This article contains supporting information online at www.pnas.org/lookup/suppl/doi:10.1073/pnas.1608568113/-/DCSupplemental.

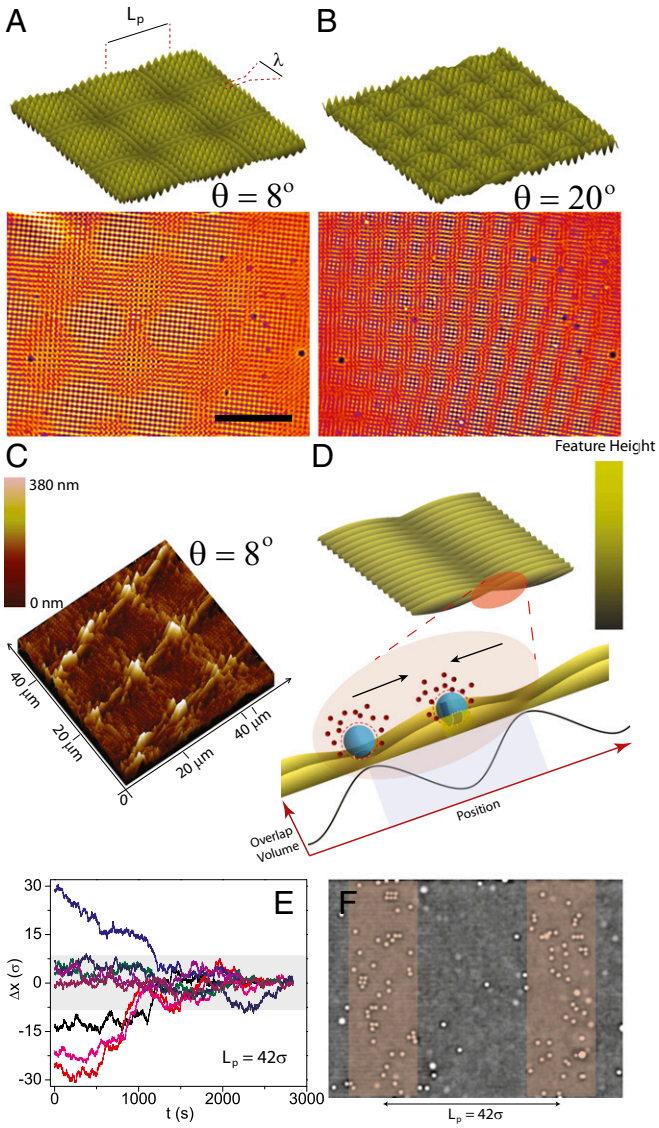

Fig. 1. Particle locomotion to traps induced by surface energy gradients. (*A* and *B*) Representative optical micrographs of square moiré patterns (*Bottom*) and the corresponding computer-generated topography maps (*Top*) for two different θs. (The scale bar in *A* represents 15 μm.) (*C*) AFM image showing modulation in trench depth for the square moiré template corresponding to *A*. (*D*) Schematic representing particle–substrate interactions on a linear moiré pattern. The overlap volume increases in the direction of the arrows and results in a net migration of particles to regions of high overlap (high E_a). (*E*) Particle trajectories on a linear moiré pattern. The gray region corresponds to regions of the pattern with high E_a. (*F*) Representative image of particle localization on moiré templates.

wavelength of the moiré pattern sets L_p, and can be independently controlled by varying θ as seen in Fig. 1 *A* and *B*. Long wavelength modulations in the feature size are also clearly evident from atomic force microscope (AFM) snapshot (Fig. 1*C*). Next, we sedimented colloidal particles [silica, diameter $\sigma = 940$ nm (22)] in the presence of a depletant polymer (sodium carboxylmethyl cellulose, $R_g = 60$ nm) on these substrates. Particle diffusion on templated surfaces has an activated form, $D = D_0 e^{-E_a/k_BT}$, where E_a is the barrier height, D_0 is the attempt frequency, and k_BT is the thermal energy (4). Apart from the polymer concentration c, the strength of the depletion attraction between the colloids and the substrate is also proportional to the excluded overlap volume that is freed up when they come in contact (23). Thus, on moiré patterns, gradients in trench (hole) depths induced gradients in E_a for the diffusing colloids and results in particle migration to the nearest energy minima (Fig. 1*D* and Movie S1).

We confirmed the enhancement in particle mean-free paths by analyzing the motion of individual particles on a linear moiré substrate, with $L_p = 42\sigma$ (Fig. 1*E* and *SI Appendix*, Fig. S1). The gray-shaded region in Fig. 1*E* represents regions of the template with a high E_a. Whereas the particles that land within this region stay localized, those that land outside (regions of low E_a) migrate nearly 25σ to the high E_a regions and are subsequently trapped. On a linear array of trenches (no surface energy gradients) and for the same c and λ as the moiré templates, we found $L \sim 5-7\sigma$ (*SI Appendix*, Fig. S2 and Movie S2). Fig. 1*F* shows a snapshot of particles localized in trap sites on moiré templates. By quantifying the variation in D across L_p, we estimated $\Delta E_a \sim 0.5 k_BT$ (*SI Appendix*, Fig. S3).

Nucleation Control on Linear Moiré Templates. The accumulation of particles in traps also increased the likelihood of crystal nucleation events at these sites. For site-specific nucleation to occur with a high fidelity, however, an optimal balance between F and the particle surface mean-free path, albeit enhanced here, is needed (4, 12). Fig. 2 *A* and *B* shows representative snapshots of crystals grown on linear moiré templates with $L_p = 42\sigma$ at identical c and surface coverage, Θ, and for two different Fs, respectively. At the smaller F, particles were able to migrate to traps before encountering arriving monomer(s) and the crystals formed are compact and confined to trap sites (Fig. 2*A* and Movie S3). For the higher F, however, this is not the case and the crystals within the traps are more ramified; colloidal islands with sixfold symmetry (highlighted by circles in Fig. 2*B* and Movie S3) nucleate outside the traps as well. We parametrized the fidelity of nucleation events at trap sites by the nucleation control efficiency (NCE), $x_{NCE} = N_m/N_{Tot}$. Here, N_m is the subset of particles that migrated to traps in a time interval Δt and then crystallized and N_{Tot} is the total number of particles that landed outside traps over the same time interval (24, 25). We note that x_{NCE} in ref. 24 is defined as the ratio of number of traps to the number of islands. This definition, however, poses difficulties in estimating x_{NCE} for spatially extended traps that can support multiple stable nuclei in the early stages of film growth, as is the case here. x_{NCE}, defined here, not only circumvents this limitation but also allows for direct comparison with previous experiments.

Next, we carried out thin-film growth experiments on linear moiré templates for different c, F, and L_p values (Movies S2 and S3). To succinctly capture the dependence of x_{NCE} on these parameters and to isolate the contribution arising from the enhancement in mean-free paths, we plotted x_{NCE} versus $p^* = L_p/L$. Here, L is the mean-free path of particles under identical experimental conditions but in the absence of energy gradients. L was obtained by measuring the density of critical clusters, n_c, at the onset of coalescence (*SI Appendix*, Fig. S2). An island with i particles is termed a critical cluster if the addition of another particle makes it stable against disintegration. We found $i = 2$ with and without surface energy gradients (*SI Appendix*, Fig. S4 and Table S1). In Fig. 2*C*, we compare x_{NCE} versus p^* from our experiments with simulation and experimental results for site-specific nucleation and growth of organic molecules (24). The data points denoted by 1 and 2 correspond to Fig. 2 *A* and *B*, respectively. Strikingly, as opposed to previous studies where complete nucleation control ($x_{NCE} = 1$) (24) was possible only for $p^* \leq 1$, on moiré patterns $x_{NCE} \approx 1$ until $p^* = 6$ and beyond which it decreases. Further, the lateral flux of particles to traps on moiré templates also effectively reduced the time taken to complete the nucleation process (*SI Appendix*, Fig. S5).

Nucleation Kinetics and Island Growth on Square Moiré Templates. The above findings clearly exemplify the efficacy of our approach in achieving site-specific nucleation for colloidal particles over a

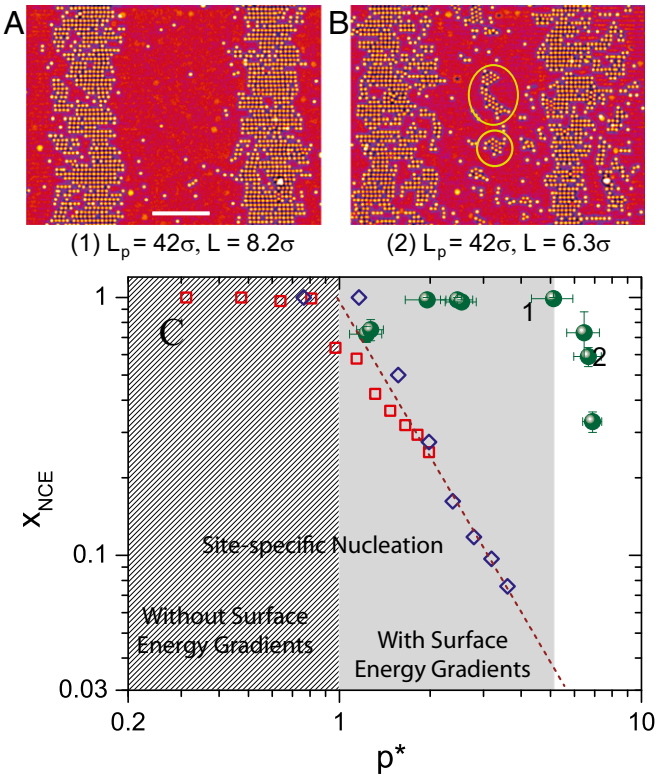

Fig. 2. Nucleation control on moiré patterns.(*A* and *B*) Representative images of crystals growth on linear moiré patterns at constant *c* and for two different *F*s. Because $\lambda = \sigma$, the templates promoted the growth of crystals with square symmetry. (*B*) Loss of nucleation control results in the nucleation of hexagonally ordered crystallites outside of the traps and is highlighted by circles. (*C*) Comparison of x_{NCE} versus p^* for conventional site-specific nucleation studies and on moiré patterns. The red and blue squares correspond to experiments and simulation results for vapor deposition of organic molecules (24). Here, nucleation control is lost ($x_{NCE} < 1$) beyond the striped region. The green circles correspond to colloid experiments on linear moiré patterns for various L_p, *c*, and *F* values. Owing to the enhancement in particle mean-free path on these substrates, $x_{NCE} < 1$ only for $p^* > 6$.

range of L_p values. To shed light on the nucleation kinetics, we mimicked atomic heteroepitaxy experiments (26–28) and measured n_c as a function of *c*, at constant *F*, on square moiré patterns with $L_p = 16\sigma$ (Movie S4). Here, *c* plays the role of an inverse temperature. At the largest *c*s studied ($c \geq 0.27$ mg/mL), particles are unable to overcome the energy barriers for surface diffusion even in the low E_a regions and the moiré template thus acts like a homogeneous surface. On such surfaces, for small *D*, atomic and colloid experiments follow rate equation predictions and find that n_c depends only on Θ and saturates to a constant, $n_c \approx 0.03$ for $i = 1$ (4, 27). This was indeed found to hold in our experiments as well (triangles in Fig. 3*A*). For $0.2 < c < 0.27$ mg/mL, although particles diffuse, their mean-free path remains smaller than L_p and nucleation events continue to occur at random locations (panel labeled "3" in Fig. 3*A*). Akin to the behavior on a homogeneous surface n_c versus *c* exhibits an Arrhenius-like dependence. We found a second plateau in n_c for *c* lying between 0.1 – 0.2 mg/mL (green squares and red circle in Fig. 3*A*). In this regime, particles perceive the heterogeneous nature of the surface energy landscape and thus their diffusivities are preferentially smaller at trap sites, which subsequently resulted in site-specific nucleation (panel 2 in Fig. 3*A*). Finally, for the lowest *c*s studied ($c \leq 0.1$ mg/mL), particles are oblivious to the underlying surface topography and n_c decreases owing to an increase in the critical cluster size ($i \geq 4$) (panel 1 in Fig. 3*A*).

Although the overall shape of the nucleation curve (red line in Fig. 3*A*) for colloids is strikingly similar to that seen for atoms (27, 28), there are fundamental differences. The black line in the schematic in Fig. 3*B* shows n_c versus D/F, or the scaled $1/T$, for homogeneous surface growth. When dimers are stable and also immobile, the rate equation predicts and experiments find that $L \propto (D/F)^{1/6}$ for $D/F > 10^4$ (4). However, for $D/F \leq 10^4$, the regime accessible in colloid experiments, *L* saturates with decreasing D/F (4, 10). For site-specific nucleation studies, which are typically performed at a fixed *F*, a plateau in n_c begins when $L \sim L_p$ (black solid circle in Fig. 3*B*) and continues until particles fail to feel the underlying substrate. More importantly, the plateau is restricted only to the yellow-shaded region, corresponding to $L \geq L_p$, of Fig. 3*B*. On moiré templates, however, the enhancement in particle mean-free path due to surface energy gradients corresponds to a larger effective D/F and the plateau in n_c should therefore lie below the homogeneous nucleation curve (blue-shaded region of Fig. 3*B*). Fig. 3*A* also shows the n_c expected for homogeneous nucleation (magenta circles in Fig. 3*A*) for D/F values corresponding to the plateau region in the nucleation curve (blue-shaded region in Fig. 3*A*) (4). The spatially averaged *D* on square moiré templates has been used while estimating D/F (*SI Appendix*, Fig. S6). In line with expectations, n_c on moiré template lies below the homogeneous nucleation curve (Fig. 3*A*).

In the plateau regime of n_c, because crystalline islands are periodically spaced and have nearly identical monomer capture rates, the island size distribution is expected to be narrower than on a homogeneous surface (4, 27). We measured the island size distribution on square moiré patterns with $L_p = 32\sigma$ by clustering particles based on their local bond-order parameter (Fig. 3C, *Inset*) and compared it with homogeneous surface growth experiments for the same Θ (*SI Appendix*, Fig. S7) (10). Whereas we found a broad range of island sizes on homogeneous surfaces (black circles in Fig. 3*D*) (10), on moiré templates the distribution was peaked with a maximum that roughly coincided with the trap size (green circles in Fig. 3*D*). Further, at the same $\Theta \sim 50\%$, we found islands on moiré templates to be more compact with a fractal dimension $d_f \sim 2$ whereas on the homogeneous surface we found $d_f \sim 1.7$ in agreement with theoretical predictions (green and black circles in Fig. 3*E*, respectively) (12). With continued particle deposition, crystals with hexagonal order nucleated and grew outside the traps and subsequent layers were found to be in registry with the underlying symmetry (*SI Appendix*, Fig. S8). We found this to be true even on templates with complex moiré periodicities. Fig. 3*F* shows a representative image of the third layer of crystals grown on a template that was fabricated by making multiple imprints at different θs. The symmetry and the width of the crystals reflect the underlying substrate periodicity with a motif: 8 $\sigma\square \rightarrow$ 8 $\sigma\hexagon \rightarrow$ 8 $\sigma\square \rightarrow$ 4 $\sigma\hexagon$.

Conclusions

Collectively, nontrivial substrate topographies, realized via a relatively simple approach, in the presence of short-range depletion interactions transported particles to desired locations and helped achieve site-specific nucleation with high fidelity even for micrometer-sized colloidal particles. Depletion interactions being sensitive only to the local geometry (29–31), a feature already exploited here, we believe our approach offers unparalleled opportunities in directing the self-assembly of complex colloids irrespective of their surface chemistry and composition (32–34). The idea outlined here, however, is far more generic. By suitable manipulation of energy barriers for surface diffusion, control over nucleation density can be exercised over a substantially broader range of *D* and *F* values. It is well-known in atomic heteroepitaxy that strain fields around misfit dislocations lead to directional adatom currents (35, 36). It is tempting to speculate if this can be exploited to guide growth for small D/F values. In the context of

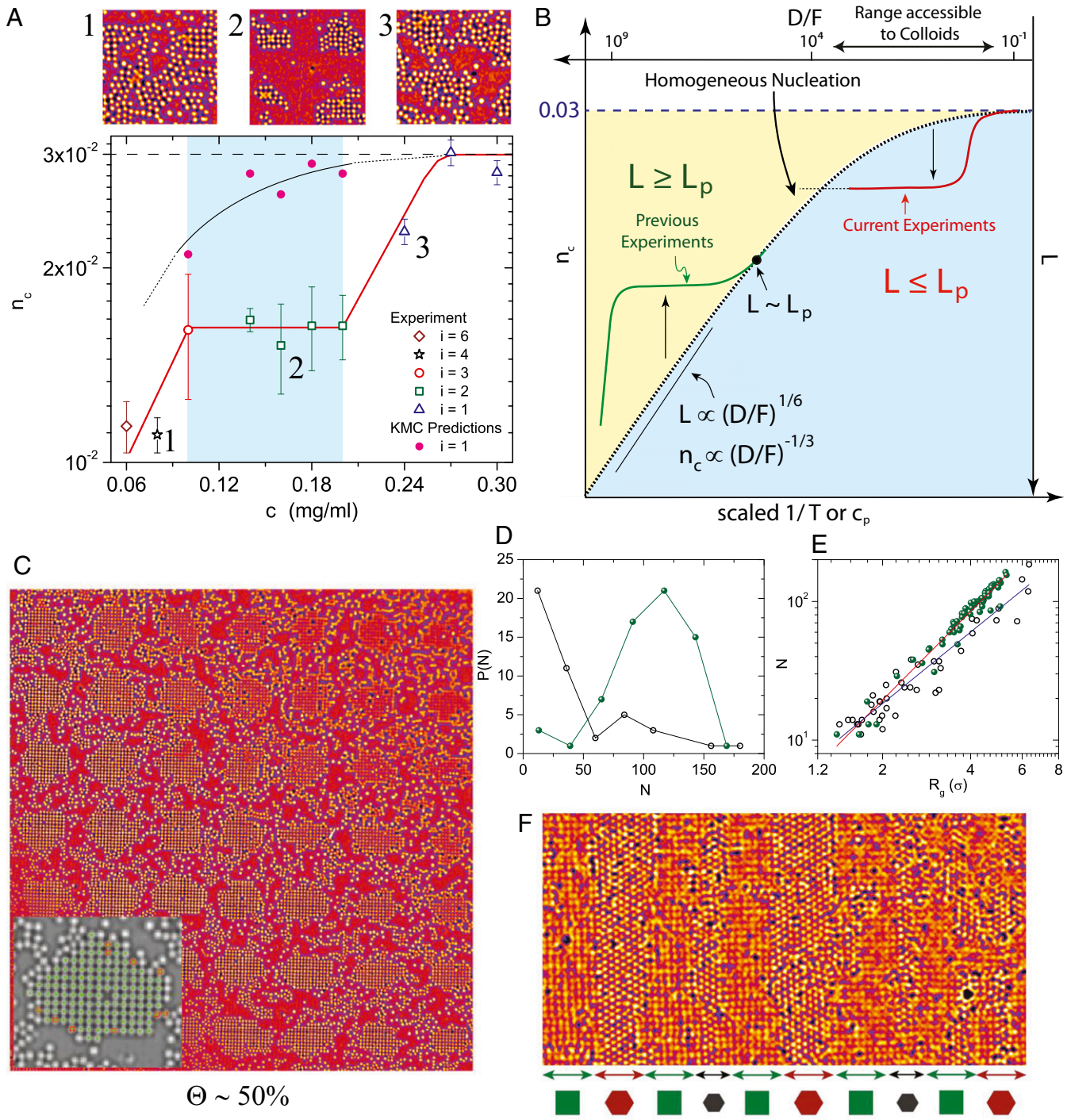

Fig. 3. Nucleation and island growth on square moiré patterns. (*A*) n_c versus c at fixed F. The legends represent the size of the critical cluster. The red line is a guide to the eye. The blue-shaded region corresponds to the regime of organized growth. The magenta circles within the blue-shaded region represent the expected n_c from homogeneous nucleation for D/F s in the plateau region (4). (*B*) Schematic of nucleation curves for homogeneous nucleation (black curve) and heterogeneous nucleation with and without energy gradients shown by red and green curves, respectively. Mean-field scaling predictions for L and n_c for $D/F > 10^4$ are also shown. (*C*) Representative snapshot of island growth on square moiré patterns with $L_p = 32\sigma$. (*Inset*) Particles clustered based on their bond-order parameter. Green represents particles with $\Psi_4 > 0.7$, and red represents particles with $\Psi_6 > 0.7$. (*D* and *E*) Island size distributions and fractal dimensions on square moiré patterns (green circles) and on hexagonal array of holes (10) (black circles) for $\Theta = 50\%$, respectively. (*F*) Colloidal crystal heterostructures grown on moiré templates. The image corresponds to the third layer of particles from the template. The size of the squares and hexagons represents the width of the strip.

nanoparticles, techniques for creating binding energy gradients by controlling the density of ligands on the surface already exist (37). In light of our findings, we believe this approach should now be exploited in guiding the self-assembly of nanoparticles as well.

Materials and Methods

Fabrication of Moiré-Patterned Templates. The templates were fabricated using the replica imprinting technique with a blazed diffraction grating (Thorlabs, 1,200 lines per millimeter, blazed angle 36.8°) chosen as the master

PHYSICS

template (8, 21). To promote the growth of crystals of various symmetries, the grating pattern was transferred to polydimethylsiloxane (PDMS, SYLGARD 184), a soft elastomer film, and was uniaxially stretched to the required spacing. For the present work, the grating periodicity on PDMS, λ, was chosen to be the same as the particle diameter $\sigma = 940$ nm, which promoted the growth of crystals of square symmetry. Using glass coverslips (#1 1/2, Electron Microscopy Sciences) as the support, the linear grating pattern in PDMS was transferred to the UV light curable optical adhesives (Norland, #68). These substrates were subsequently used as the hard master template for further imprinting process. Next, a PMMA (Sigma, mol wt 120,000) layer was spin-coated (at ~1,000 rpm) on a glass coverslip to a thickness of ~500 nm using standard protocols. The PMMA-coated coverslips were pressed against the linear grating on the UV glue patterns which was premaintained at a temperature $T_1 \sim 126° > T_g$. Here, T_g is the glass transition temperature of PMMA. This transferred the linear grating patterns to the PMMA. A subsequent second imprint at a temperature $T_2 \sim 122° (< T_1)$ and at an angle $\theta \leq 45°$ relative to the first resulted in a linear moiré pattern. Typically, θ was varied between $0° < \theta < 20°$. To fabricate square moiré patterns, we first fabricated a template with square symmetry by setting $\theta = 90°$ between the first and second imprints. We then followed the procedure used for fabricating linear moiré patterns. The multiple transfer processes involved in the fabrication of square moiré templates resulted in a decrease in the groove depth and the yield of working templates was lower than linear moiré patterns. However, improvements in the imprinting technique such as starting with square patterns with larger groove depth can enormously improve the yield of square moiré templates.

To enable comparison of the nucleation kinetics for various depletion concentrations *c* and deposition fluxes *F*, experiments were carried out on the same template. To this end, we fabricated glass flow cells, like in the work of Ganapathy et al. (10), where the bottom of the flow cell is a PMMA-coated glass coverslip having the required template. The height of the flow cell was ~1.3 mm. The flow cell was filled with a 1:1 mixture of dimethyl sulfoxide (Merck) and water containing the requisite amounts of NaCMC and silica colloids. *D* was tuned by varying *c*, and *F* by varying the volume fraction of colloids. Particles were then allowed to sediment onto the substrate and the nucleation and growth kinetics were followed by optical microscopy (Leica DMI 6000B with a 100× oil immersion objective Leica, Plan-Apochromat, N.A. 1.4). Images were captured using a digital camera (Foculus 234SB) with a frame rate between 2 and 5 frames per second. To improve statistics, nucleation and growth were investigated over a substantially larger field of view using a Photron FastCam SA4 to capture individual images at suitably spaced time intervals. The images were processed using ImageJ and MATLAB, and center-of-mass coordinates of colloids were obtained using standard MATLAB algorithms (38).

The charge-stabilized spherical silica colloids were synthesized using the Stöber process and we followed the protocols established by Zhang et al. (22).

The AFM measurements were done using Veeco AFM apparatus in noncontact mode. Before the measurements, a thin layer of gold, ~20 nm, was coated on the moiré template to prevent the AFM tip from sticking to the template.

ACKNOWLEDGMENTS. We thank Arjun Yodh, Vinothan Manoharan, and Prerna Sharma for useful discussions. We thank Satyendra Nath Gupta for AFM measurements. C.K.M. thanks Hima Nagamanasa and Shreyas Gokhale for fruitful interactions. C.K.M. thanks Chemistry and Physics of Materials Unit, Jawaharlal Nehru Centre for Advanced Scientific Research (JNCASR) for financial support. A.K.S. thanks Department of Science and Technology, India for support under a J. C. Bose Fellowship, and R.G. thanks Sheikh Saqr Laboratory and International Centre for Materials Science, JNCASR for financial support.

1. Zhang Z, Lagally MG (1997) Atomistic processes in the early stages of thin-film growth. *Science* 276(5311):377–383.
2. Barth JV, Costantini G, Kern K (2005) Engineering atomic and molecular nanostructures at surfaces. *Nature* 437(7059):671–679.
3. Shchukin VA, Bimberg D (1999) Spontaneous ordering of nanostructures on crystal surfaces. *Rev Mod Phys* 71(4):1125.
4. Brune H (1998) Microscopic view of epitaxial metal growth: Nucleation and aggregation. *Surf Sci Rep* 31(4):125–229.
5. Brune H, Giovannini M, Bromann K, Kern K (1998) Self-organized growth of nanostructure arrays on strain-relief patterns. *Nature* 394(6692):451–453.
6. Aizenberg J, Black AJ, Whitesides GM (1999) Control of crystal nucleation by patterned self-assembled monolayers. *Nature* 398(6727):495–498.
7. Van Blaaderen A, et al. (1997) Template-directed colloidal crystallization. *Nature* 385(6614):321–324.
8. Lin Kh, et al. (2000) Entropically driven colloidal crystallization on patterned surfaces. *Phys Rev Lett* 85(8):1770–1773.
9. Kim SH, Lee SY, Yang SM, Yi GR (2011) Self-assembled colloidal structures for photonics. *NPG Asia Mater* 3(1):25–33.
10. Ganapathy R, Buckley MR, Gerbode SJ, Cohen I (2010) Direct measurements of island growth and step-edge barriers in colloidal epitaxy. *Science* 327(5964):445–448.
11. Savage JR, et al. (2013) Entropy-driven crystal formation on highly strained substrates. *Proc Natl Acad Sci USA* 110(23):9301–9304.
12. Jensen P, Barabási AL, Larralde H, Havlin S, Stanley HE (1994) Deposition, diffusion, and aggregation of atoms on surfaces: A model for nanostructure growth. *Phys Rev B Condens Matter* 50(20):15316–15329.
13. Cho SY, Jeon HJ, Kim JS, Ok JM, Jung HT (2014) Hierarchical ordering of quantum dots and liquid with tunable super-periodicity into high aspect ratio moiré superlattice structure. *Adv Funct Mater* 24(44):6939–6947.
14. Chen ZG, et al. (2012) Two-dimensional crystallization of hexagonal bilayer with Moiré patterns. *J Phys Chem B* 116(14):4363–4369.
15. Zheng H, et al. (2002) Two component particle arrays on patterned polyelectrolyte multilayer templates. *Adv Mater* 14(8):569.
16. Kim E, Xia Y, Whitesides GM (1996) Micromolding in capillaries: Applications in materials science. *J Am Chem Soc* 118(24):5722–5731.
17. Kim H, et al. (2009) Structural colour printing using a magnetically tunable and lithographically fixable photonic crystal. *Nat Photonics* 3(9):534–540.
18. Cheng Z, Russel WB, Chaikin P (1999) Controlled growth of hard-sphere colloidal crystals. *Nature* 401(6756):893–895.
19. Dziomkina NV, Vancso GJ (2005) Colloidal crystal assembly on topologically patterned templates. *Soft Matter* 1(4):265–279.
20. Wang D, Möhwald H (2004) Template-directed colloidal self-assembly–the route to "top-down" nanochemical engineering. *J Mater Chem* 14(4):459–468.
21. Xia Y, et al. (1996) Complex optical surfaces formed by replica molding against elastomeric masters. *Science* 273(5273):347–349.
22. Zhang L, et al. (2009) Hollow silica spheres: Synthesis and mechanical properties. *Langmuir* 25(5):2711–2717.
23. Asakura S, Oosawa F (1954) On interaction between two bodies immersed in a solution of macromolecules. *J Chem Phys* 22(7):1255–1256.
24. Wang WC, et al. (2007) Patterned nucleation control in vacuum deposition of organic molecules. *Phys Rev Lett* 98(22):225504.
25. Kalischewski F, Heuer A (2009) Dynamic effects on the loss of control in template-directed nucleation. *Phys Rev B* 80(15):155421.
26. Haas G, et al. (2000) Nucleation and growth of supported clusters at defect sites: Pd/mgo (001). *Phys Rev B* 61(16):11105.
27. Rohart S, Baudot G, Repain V, Girard Y, Rousset S (2005) Site selective nucleation on surfaces: The rate equation model compared with VT-STM experiment of Co on Au (788). *J Cryst Growth* 275(1):e203–e209.
28. Rousset S, et al. (2005) Self-organized epitaxial growth on spontaneously nano--patterned templates. *C R Phys* 6(1):33–46.
29. Sacanna S, Irvine WT, Chaikin PM, Pine DJ (2010) Lock and key colloids. *Nature* 464(7288):575–578.
30. Chen Q, Bae SC, Granick S (2011) Directed self-assembly of a colloidal kagome lattice. *Nature* 469(7330):381–384.
31. Rossi L, et al. (2011) Cubic crystals from cubic colloids. *Soft Matter* 7(9):4139–4142.
32. Manoharan VN, Elsesser MT, Pine DJ (2003) Dense packing and symmetry in small clusters of microspheres. *Science* 301(5632):483–487.
33. Manoharan VN (2015) COLLOIDS. Colloidal matter: Packing, geometry, and entropy. *Science* 349(6251):1253751.
34. Kim M, Anthony SM, Granick S (2009) Activated surface diffusion in a simple colloid system. *Phys Rev Lett* 102(17):178303.
35. Schroeder M, Wolf D (1997) Diffusion on strained surfaces. *Surf Sci* 375(1):129–140.
36. Larsson M, Cho K, Clemens B (2004) Surface diffusion mechanisms for strain-induced self-assembly. *Phys Rev B* 69(15):155426.
37. Genzer J (2012) Surface-bound gradients for studies of soft materials behavior. *Annu Rev Mater Res* 42:435–468.
38. Crocker JC, Grier DG (1996) Methods of digital video microscopy for colloidal studies. *J Colloid Interface Sci* 179(1):298–310.